The Journal of Chemical Physics

Extracting the sample response function from experimental two-dimensional terahertz-infrared-visible spectra

Cite as: J. Chem. Phys. **158**, 134201 (2023); https://doi.org/10.1063/5.0138442
Submitted: 12 December 2022 • Accepted: 13 March 2023 • Accepted Manuscript Online: 13 March 2023 • Published Online: 04 April 2023

Pankaj Seliya, Mischa Bonn and Maksim Grechko

The Journal of Chemical Physics ARTICLE scitation.org/journal/jcp

Extracting the sample response function from experimental two-dimensional terahertz-infrared-visible spectra

Cite as: J. Chem. Phys. 158, 134201 (2023); doi: 10.1063/5.0138442
Submitted: 12 December 2022 • Accepted: 13 March 2023 •
Published Online: 4 April 2023

Pankaj Seliya, Mischa Bonn, and Maksim Grechko[a)]

AFFILIATIONS

Department of Molecular Spectroscopy, Max Planck Institute for Polymer Research, Ackermannweg 10, D-55128 Mainz, Germany

Note: This paper is part of the JCP Special Topic on Celebrating 25 Years of Two-dimensional Infrared (2D IR) Spectroscopy.
[a)]**Author to whom correspondence should be addressed:** grechko@mpip-mainz.mpg.de

ABSTRACT

Terahertz molecular motions are often probed by high-frequency molecular oscillators in different types of non-linear vibrational spectroscopy. Recently developed two-dimensional terahertz-infrared-visible spectroscopy allows direct measuring of this coupling and, thus, obtaining site-specific terahertz vibrational spectrum. However, these data are affected by the intensity and phase of the employed laser pulses. In this work, we develop a method of extracting sample response—representing solely physical properties of a material—from experimental spectra. Using dimethyl sulfoxide as a model molecule to verify this method, we measure the coupling between C–H stretch vibration of its methyl groups and terahertz intramolecular twist and wagging modes.

INTRODUCTION

Molecular low-frequency vibrational modes (LFMs) in the terahertz (THz) frequency range can play a role in (bio-) chemical processes in condensed phases at room temperature.[1–4] Non-linear mid-infrared (MIR) spectroscopy techniques (transient absorption and 2D IR) measure high-frequency vibrational modes (HFMs) to obtain insight into these motions at locations of specific chemical groups.[5–10] Such measurements probe terahertz dynamics indirectly via LFM-HFM coupling, by exciting and probing only a high-frequency oscillator. Sophisticated relations between the HFM frequency/transition dipole moment and the LFM coordinate complicate determining the relevant LFM modes from such measurements. Recently, we have developed two-dimensional terahertz-infrared-visible (2D TIRV) spectroscopy to measure LFM-HFM coupling directly.[11,12] This technique can identify the relevant LFMs using mid-infrared spectroscopy selectivity, thereby disentangling the typically broad featureless low-frequency spectral response.[13–16] Previously, we have used this technique to study the coupling between intra- and inter-molecular motions in liquid water and the coupling between phonon vibrations and N–H stretch vibrations in hybrid perovskites.[11,12] However, taking full advantage of the 2D TIRV spectroscopy requires extracting the system's complex-valued third-order non-linear response function $S^{(3)}$ from the measured data.

A measured 2D TIRV spectrum is determined by a product of $S^{(3)}$ and spectra of laser pulses. The latter can be considered as an instrument response function (IRF), which affects both the intensity and phase of the 2D spectrum. Deriving $S^{(3)}$, which contains the physical properties of a sample, thus requires eliminating IRF from the experimental data. This requirement is analogous to data processing in other non-linear spectroscopy techniques where the signal depends on the intensities and phases of the employed laser pulses. For example, the progress in 2D IR and 2D electronic spectroscopy was enabled by a method of determining the phase of a spectrum.[17–21] The method utilizes the equality of 2D spectrum projection and transient absorption spectrum. Another technique, phase-resolved sum-frequency generation (PR SFG) spectroscopy, uses the response of reference material to obtain the second-order response function of a

sample.[22,23] Here, we develop a similar method for 2D TIRV spectroscopy.

We have recently reported a procedure that allows separating different excitation pathways in 2D TIRV spectroscopy.[24] This was a critical step toward deriving material response function from experimental data because different excitation pathways produce signals via different mixing of the terahertz and infrared fields: sum- and difference-frequency mixing. Here, we report a method to eliminate the effect of the laser fields and obtain the spectrum of sample response function in 2D TIRV spectroscopy. To this end, we utilize a thin (1 μm) silicon nitride (SiN_x) membrane as the reference material. Its response gives a spectrum that directly reflects the distribution of intensities and phases of all the laser pulses used in 2D TIRV spectroscopy to generate and detect signal field. We demonstrate the approach on a model sample, liquid dimethyl sulfoxide (DMSO), which has intense low- and high-frequency modes that are sufficiently strongly coupled to generate a substantial 2D TIRV signal.

PRINCIPLES OF 2D TIRV SPECTROSCOPY

The theoretical formalism and experimental implementation of 2D TIRV spectroscopy have been discussed in detail elsewhere.[11,24,25] In brief, in a 2D TIRV spectroscopy measurement, four-wave mixing of a narrowband visible (VIS), and broadband terahertz (THz) and mid-infrared (IR) pulses induce the emission of a signal field by a sample (Fig. 1). The resonant interactions of THz and IR pulses with the sample excite its LFMs and HFMs, respectively, with time delay τ between the pulses. VIS pulse adds third, non-resonant interaction between electromagnetic field and material to enable signal generation from isotropic media. Also, using VIS pulses leads to the signal being emitted in the visible frequency range, typically 620–720 nm, for which sensitive detectors are commercially available. Doubly resonant generation of signal—via excitation of both LFMs and HFMs—requires a two-quantum transition at one of the excitation steps and, thus, coupling between the modes. The signal field is dispersed in a spectrometer and measured using its interference with a local oscillator (LO) pulse at different time delays τ between the THz pulse and IR/VIS pulse pair. Fourier transformation of the time-domain data over τ provides the THz frequency axis (ω_1), representing LFMs. The second frequency axis, ω_2, representing HFMs, is obtained by subtracting the frequency of the VIS pulse from the spectrometer frequency. A constant time delay $\delta \approx 4.1$ ps between the signal and LO pulses is used to distinguish positive and negative ω_2 frequencies and separate signals generated by rephasing (VIS + IR−THz difference-frequency mixing) and non-rephasing (VIS + IR + THz sum-frequency mixing) excitation pathways (quadrant separation).[24] Rephasing and non-rephasing signals appear in the II/IV and I/III quadrants of the 2D spectrum, respectively.

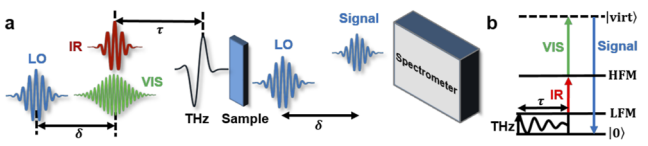

FIG. 1. (a) Scheme of experimental implementation of 2D TIRV spectroscopy. (b) Energy level diagram of a typical excitation pathway.

Assuming an infinitely small bandwidth of the VIS pulse, a measured 2D TIRV spectrum Γ in quadrants I and II is given by a product[24]

$$\begin{aligned}\Gamma(\omega_2+\Omega_{VIS},\omega_1) \propto &\left\{S^{(3)}(\omega_2+\Omega_{VIS},\omega_2,\omega_1)\right.\\ &\left.+\,S^{(3)}(\omega_2+\Omega_{VIS},\omega_2,\omega_2-\omega_1)\right\}\\ &\times E_{THz}(\omega_1)E_{IR}(\omega_2-\omega_1)\\ &\times E_{VIS}(\Omega_{VIS})E_{LO}(-\omega_2-\Omega_{VIS})e^{i(\omega_2+\Omega_{VIS})\delta}. \quad (1)\end{aligned}$$

Here, $S^{(3)}$ is the third-order response function of a sample, which reflects its physical properties; E_{VIS} is the complex-valued spectral amplitude of the VIS electric field with frequency Ω_{VIS}; and E_{THz}, E_{IR}, and E_{LO} are complex-valued electric field spectra of THz, IR, and LO pulses, respectively. The first and second terms in Eq. (1) represent different interaction sequences between the THz and IR fields and the sample. In the first (second) term, the interaction of the sample with THz (IR) precedes interaction with IR (THz). Equation (1) shows that the intensity and phase of a measured 2D TIRV spectrum are affected by the spectral shapes and phases of the employed laser pulses. We note that the THz, IR, and LO pulse phases can have complex dependence on frequency (due to, e.g., dispersion). Hence, a measured spectrum can be considered a product of the sample response function and instrument response function (IRF), which is given by the product of electric fields.

Deriving the complex-valued spectrum of $S^{(3)}_{sample}$ requires eliminating laser fields from the product in Eq. (1). To this end, we use an approach similar to PR SFG spectroscopy.[22] In this technique, a measured spectrum Γ_{sample} of a sample is divided by a non-resonant spectrum Γ_{ref} of a reference material (typically quartz). For non-resonant interactions, a material response function of any order is real-valued and constant (frequency-independent).[26] Thus, the non-resonant spectrum is linearly proportional to the IRF of an experimental setup and $\Gamma_{sample}/\Gamma_{ref} \propto S^{(3)}_{sample}$. This approach can be employed using a resonant reference material as well, given that its response function $S^{(3)}_{ref}$ is known. In this case,

$$S^{(3)}_{sample} = \frac{\Gamma_{sample}}{\Gamma_{ref}} S^{(3)}_{ref}.$$

We demonstrate that in 2D TIRV spectroscopy, a thin silicon nitride (SiN_x) membrane is a suitable reference material to derive the complex-valued spectrum of the sample response function.

RESULTS AND DISCUSSION

We use liquid dimethyl sulfoxide (DMSO) as a model sample. The absorption spectrum of DMSO in the mid- and far-infrared frequency range is shown in Fig. 2. In the terahertz frequency range, this spectrum contains two sharp vibrational modes at 333 and 383 cm^{-1} labeled 2 and 3. These vibrations are assigned to intramolecular CH_3–CH_3 twist (υ_{23}) and wagging (υ_{11}) modes, respectively.[27–29] There is also a weak shoulder at about 308 cm^{-1} (labeled 1), which is also produced by intramolecular motion and

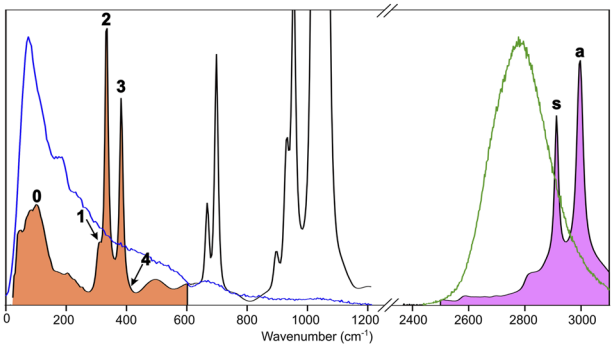

FIG. 2. Black line shows the absorption spectrum of liquid DMSO. Relevant low- and high-frequency ranges are shaded in red and purple, respectively. Intensity spectra of THz and IR laser pulses are shown by blue and green lines, respectively.

is assigned to C-S-C bending (υ_{12}).[29] Besides intramolecular vibrations, the spectrum contains intermolecular libration motion at frequencies below 150 cm^{-1} (labeled 0).[27]

Because LFMs 2 (333 cm^{-1}) and 3 (383 cm^{-1}) of DMSO displace CH_3 groups of the molecule, one can expect substantial coupling between LFMs and the C–H stretch vibrations. The C–H stretch symmetric and asymmetric vibrational modes have frequencies of 2913 and 2996 cm^{-1}, respectively (labeled with s and a in Fig. 2). Figure 3(a) shows the time-domain 2D TIRV data of DMSO measured in this IR frequency range using a femtosecond IR pulse with a bandwidth of 250 cm^{-1} and a central frequency of 2780 cm^{-1} (Fig. 2). Fourier transformation over time axis and quadrant separation yields 2D spectrum Γ_{DMSO}. Figure 3(b) shows the first and second quadrants of the absolute-value 2D TIRV spectrum ($|\Gamma_{DMSO}|$). Sum-frequency mixing of the THz and IR fields produces a signal in the first quadrant at ω_2-frequencies of CH_3 stretch vibrations.[24] The offset of the IR pulse frequency from CH_3 modes to red favors this process. The similar signal in the second quadrant is weak because it is produced by difference-frequency mixing of the IR and THz fields, which is hampered by the IR frequency offset. Instead, the second quadrant contains a signal parallel to the diagonal and intersecting ω_2-frequency axis at the CH_3 stretch frequencies.

Figures 3(c) and 3(d) show real and imaginary parts of the Γ_{DMSO}, respectively. Their shape is affected by the spectral intensities and phases of the THz, IR, and LO pulses. Inter alia, an offset of time zero in time-domain data [Fig. 3(a)] and time delay δ between signal and LO results in oscillations along ω_1 and ω_2 axes, respectively. To eliminate this effect of IRF, we measure the 2D TIRV spectrum Γ_{SiN} of a reference material, a ~1 μm thick SiN_x membrane [Figs. 3(e)–3(h)]. Because SiN_x has no resonances at mid-infrared and visible frequencies, interaction with IR and VIS pulses is non-resonant for this material. In contrast, in the far-infrared frequency range, SiN_x has intense vibrational resonances (Fig. 4). Hence, the signal can be generated by its non-resonant and resonant interaction with the THz pulse. In the former case, SiN_x response function $S^{(3)}_{SiN}$ is real-valued and constant, whereas in the latter case, it is complex-valued and depends on the ω_1-frequency,

$$S^{(3)}_{SiN}(\omega_2, \omega_1) \propto S^{(1)}_{SiN}(\omega_1).$$

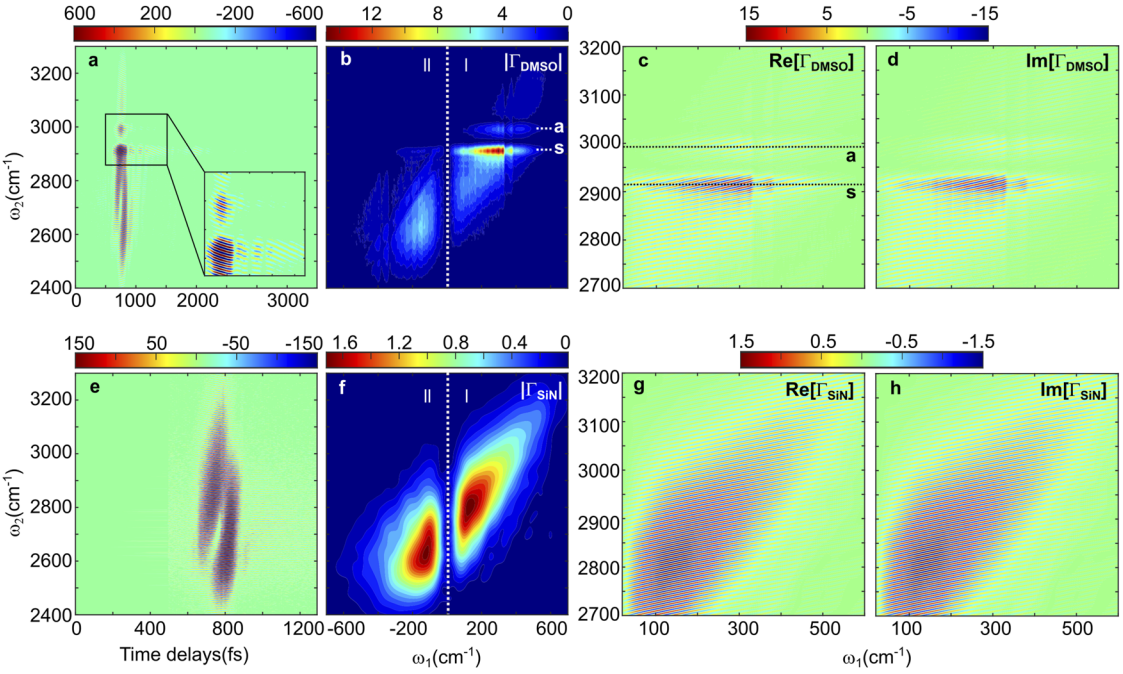

FIG. 3. Time-domain data (a), absolute value (b), real (c), and imaginary (d) parts of 2D TIRV spectrum of DMSO. Time-domain data (e), absolute value (f), real (g), and imaginary (h) parts of 2D TIRV spectrum of SiN_x, which serves as a reference. In panels (a) and (e), the time zero is arbitrarily defined as the beginning of a dataset.

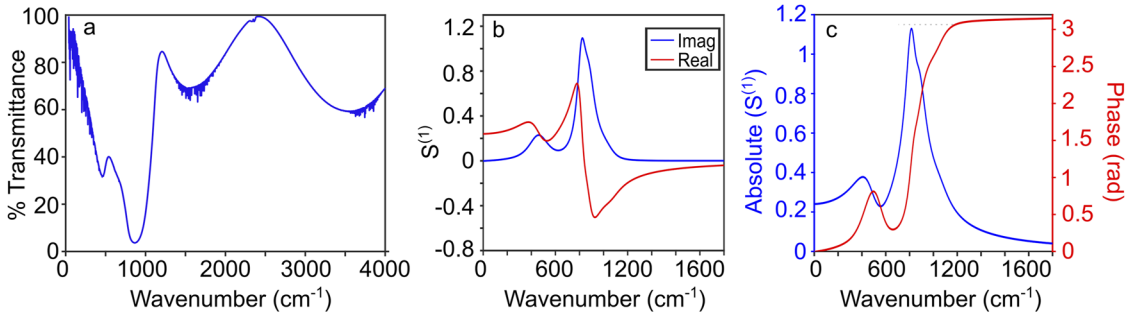

FIG. 4. (a) Transmittance spectrum of 1 μm thick SiN_x membrane. (b) Real and imaginary parts and (c) amplitude and phase of $S^{(1)}_{SiN}$.

Here, $S^{(1)}_{SiN}$ is the resonant first-order response function of SiN_x. Figure 4 shows the $S^{(1)}_{SiN}$ spectrum calculated using its reported permittivity ε_{SiN},[30]

$$S^{(1)}_{SiN}(\omega) = \frac{\varepsilon_{SiN}(\omega) - 1}{4\pi\rho_0},$$

where ρ_0 is the number density of absorbers (we assume $\rho_0 = 1$). In the 0-700 cm^{-1} THz frequency range of our 2D TIRV experiment, the $S^{(1)}_{SiN}$ amplitude varies by about 67% and its phase by up to 0.8 rad. This dispersion is primarily caused by the transverse optical phonon resonance around 825 cm^{-1}.[31]

Using SiN_x as a reference material, we test the two possible extreme cases of interaction with the THz pulse. Figures 5(a)–5(c) and 5(d)–5(f) show $S^{(3)}_{DMSO}$ in the first quadrant obtained assuming fully non-resonant (case I) and partly resonant (for the THz pulse interaction, case II) SiN_x signal generation, respectively,

$$(a-c)S^{(3)}_{DMSO}(\omega_2,\omega_1) = \frac{\Gamma_{DMSO}(\omega_2,\omega_1)}{\Gamma_{SiNx}(\omega_2,\omega_1)},$$

$$(d-f)S^{(3)}_{DMSO}(\omega_2,\omega_1) = \frac{\Gamma_{DMSO}(\omega_2,\omega_1)}{\Gamma_{SiNx}(\omega_2,\omega_1)} \cdot S^{(1)}_{SiN}(\omega_1).$$

These two assumptions produce $S^{(3)}_{DMSO}$ spectra, which are very similar for $\omega_1 \lesssim 400$ cm^{-1}. For higher ω_1-frequencies, the difference of the line shape becomes more significant because of the ~0.8 rad accumulated phase of $S^{(1)}_{SiN}$. A 2D spectrum with the correct

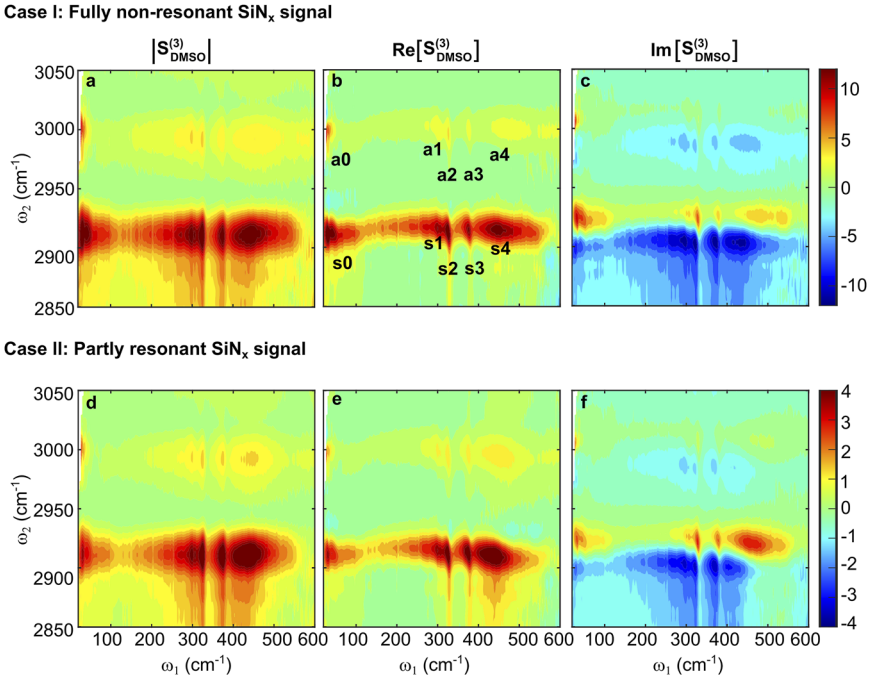

FIG. 5. (a)–(c) Absolute value, along with the real and imaginary parts of the DMSO response function spectrum, assuming fully non-resonant SiN_x signal. (d)–(f) Absolute value, along with the real and imaginary parts of the DMSO response function spectrum, assuming partly resonant SiN_x signal.

phase should fulfill the Kramers–Kronig relations (KKR) calculated parallel to one of the frequency axis,[26] for instance,

$$\mathrm{Im}\left(S^{(3)}_{\mathrm{DMSO}}(\omega_2,\omega_1)\right) = -\frac{1}{\pi}\int_{-\infty}^{+\infty}\frac{Re\left(S^{(3)}_{\mathrm{DMSO}}(\omega_2,\omega')\right)}{\omega'-\omega_1}d\omega'.$$

Figure 6 shows real and imaginary parts of the spectra in Fig. 5 taken at the symmetric stretch frequency (ω_2 = 2913 cm^{-1}, mode s in Fig. 2). For both cases I and II, there is a significant discrepancy in the frequency range below ~100 cm^{-1} between the imaginary part inferred from the real part using the KKR and experimental data [Figs. 6(b) and 6(d)]. This can be explained by two factors: low signal intensity in this spectral range and the limited spectral range (0–600 cm^{-1}) used in the calculations. The 2D TIRV signal from SiN_x reduces by a factor of ten and more at $\omega_1 \lesssim 20$ cm^{-1}, thus making unreliable intensities of the derived $S^{(3)}_{\mathrm{DMSO}}$ at these ω_1-frequencies. Because the KKR is not local, this can affect the inferred imaginary part in Fig. 6 in the frequency range significantly beyond 20 cm^{-1}. In addition, the correct KKR also requires integration over negative frequencies (quadrant II). In the calculations, we use data only from quadrant I (0–600 cm^{-1}) because of the low signal-to-noise ratio in quadrant II. This approximation can influence the inferred imaginary part, particularly at low ω_1-frequencies. Above 100 cm^{-1}, the inferred imaginary part agrees reasonably with the experimental data for case II, given that the calculated data in 500–600 cm^{-1} range can also be affected by the limited spectral range used in the KKR. For case I, the agreement between the calculated and experimental spectra is worse [Fig. 6(b)]. Thus, the 2D TIRV signal of SiN_x is generated predominantly via the resonant interaction with the THz pulse, and the correct spectrum of $S^{(3)}_{\mathrm{DMSO}}$ is given by case II.

For each of the C–H stretch vibrational modes s and a, the $S^{(3)}_{\mathrm{DMSO}}$ spectrum contains three peaks at $\omega_1 \approx$ 300, 326 and 376 cm^{-1} (s1, s2, s3 and a1, a2, a3 in Fig. 5) reflecting their coupling with the intramolecular LFMs 1, 2, and 3. We attribute the additional prominent peaks s4 and a4 to an LFM with a weak transition dipole moment and strong coupling with C–H stretch vibrations. This weakly absorbing mode is obscured in the absorption spectrum in Fig. 2. To determine which of the THz-IR and IR-THz interaction sequences produces these signals, we perform a Fourier transformation of the spectrum over the ω_1-frequency axis back into the time domain [Fig. 7(a)]. Because the data processing eliminates phases of the laser pulses, $S^{(3)}_{\mathrm{DMSO}}$ has a maximum at $t = 0$ (note that here the t-axis is uniquely determined by the phase of the frequency-domain spectrum). We use a square window function to select data at negative ($t < 0$) and positive ($t > 0$) time and perform their Fourier transformation separately to derive the signal generated by the IR-THz and THz-IR interaction sequences, respectively. The spectrum of the signal at $t < 0$ contains peaks that are broad over the ω_1 axis and narrow over the ω_2 axis [Figs. 7(b)–7(d)]. Thus, the IR-THz interaction sequence is resonant for the IR interaction and presumably non-resonant for the THz interaction. In contrast, the spectrum of $t > 0$ contains a signal generated by the coupled intramolecular LFMs and C–H stretch vibrations [Figs. 7(e)–7(g)]. Hence, the doubly resonant signal is produced by DMSO molecules interacting first with the THz pulse, followed by interaction with the IR pulse.

Cross-peaks between CH_3 stretch vibrations and intramolecular LFMs 1, 2, and 3 are at frequencies of $\omega_1 \approx$ 300, 326, and 376 cm^{-1}. These frequencies are systematically lower by about 5 cm^{-1} than LFMs locations in the absorption spectrum (accuracy of the ω_1 and ω_2 frequencies is about 1 cm^{-1} each; see the supplementary material for details). This deviation cannot be

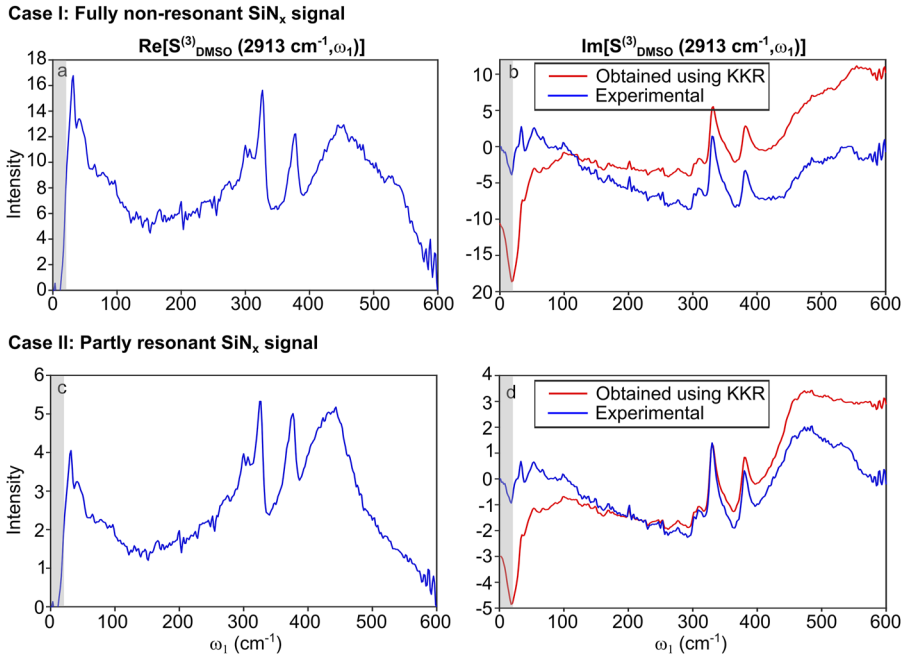

FIG. 6. Real (a) and imaginary (b) parts of $S^{(3)}_{\mathrm{DMSO}}(2913\,\mathrm{cm}^{-1},\omega_1)$, assuming fully non-resonant SiN_x signal. Real (c) and imaginary (d) parts of $S^{(3)}_{\mathrm{DMSO}}(2913\,\mathrm{cm}^{-1},\omega_1)$, assuming partly resonant SiN_x signal. Blue lines show experimental data, and red lines show the imaginary part calculated from the corresponding real part using the Kramers–Kronig relation.

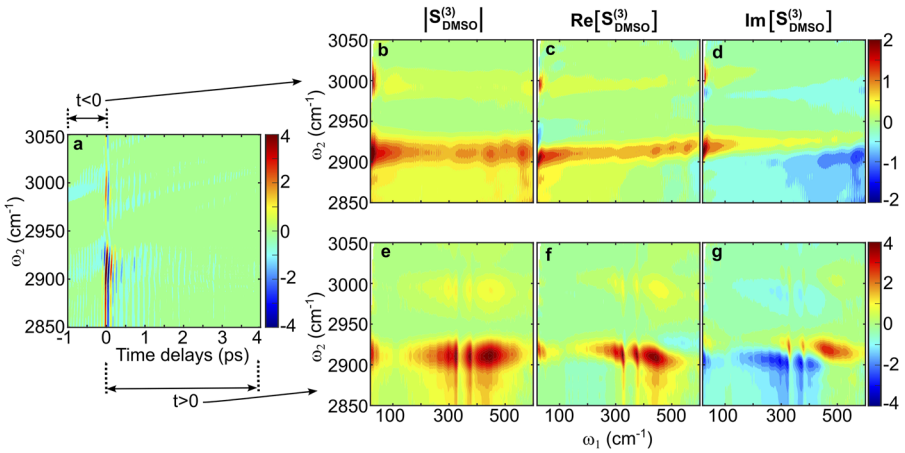

FIG. 7. (a) Time-domain data obtained by the inverse Fourier transformation of $S^{(3)}_{DMSO}(\omega_2, \omega_1)$ over ω_1 frequencies. (b) Absolute value, (c) real, and (d) imaginary parts of the spectrum obtained by Fourier transformation of the signal for $t < 0$ in (a). (e) Absolute value, (f) real, and (g) imaginary parts of the spectrum obtained by Fourier transformation of the signal for $t > 0$ in (a).

explained by different frequencies of LFMs in the excited state of the C–H oscillator because the THz pulse excites LFMs in the ground vibrational state of the C–H stretch. Because the first excited state of the DMSO low-frequency intramolecular vibrations is populated at room temperature, the THz pulse excites molecules also from the first to the second excited state. One can hypothesize a significantly stronger coupling between the second excited state of THz modes and C–H stretch vibrations, which can dominate the 2D TIRV spectrum. Thus, the $\approx 5\ cm^{-1}$ offset of resonances in the 2D TIRV spectrum along the ω_1-axis can stem from the own mechanical anharmonicity of DMSO intramolecular vibrations. To verify this hypothesis, we measure the absorption spectrum of the DMSO in a 1 mm thick sample cell to identify possible overtone transitions of the molecule in the THz frequency range (Fig. S4 in the supplementary material). A weak resonance at about 765 cm^{-1} can be tentatively assigned to the overtone transition of the 383 cm^{-1} vibrational mode, which implies $\approx 1\ cm^{-1}$ own mechanical anharmonicity of this LFM. An alternative explanation of the red-shifted response can be a slight inhomogeneous broadening of the LFMs. For instance, LFM frequencies can have a weak dependence on the instantaneous conformation of DMSO molecules, such as the rotational orientation of its methyl groups around S–C bonds. Assuming LFM-HFM interaction strength also depends on instantaneous DMSO conformation, this can lead to stronger coupling between red-shifted LFM oscillators and C–H stretch vibrations. Hence, an offset of resonance frequencies in the 2D TIRV spectrum can occur as compared to linear absorption. However, a comprehensive explanation of this phenomenon requires accurate theoretical calculations.

At even lower ω_1 frequency, the $S^{(3)}_{DMSO}$ spectra display coupling between the C–H stretch vibration and intermolecular librational motions [s0 and a0 in Fig. 5(b)]. The librational motion changes the spatial orientation of the C–H stretch transition dipole moment, and because the intermolecular forces on the CH_3 groups are typically rather weak, this coupling is likely produced by predominantly electrical anharmonicity. The maximum intensity in the 2D spectrum is substantially below a THz frequency of 100 cm^{-1}—the maximum of linear absorption (Fig. 2). We hypothesize that this can be due to the larger amplitude (angle) of libration at lower frequencies and, thus, stronger LFM-HFM coupling.

In summary, we present a method of deriving a complex-valued sample response function in experimental 2D TIRV spectroscopy. The sample response free from the instrument response function reflects its physical properties and can be directly compared with theoretical calculations. For a model liquid DMSO sample, we directly measure the coupling between high-frequency C–H stretch modes and THz molecular motions, both intramolecular vibrations and intermolecular libration. These results pave the way for the utilization of 2D TIRV spectroscopy for the quantitative study of vibrational dynamics in liquids and soft materials important in different fields of chemistry.

METHODS

The experimental setup is described in detail elsewhere.[24] Here, we provide a brief overview. The output of a femtosecond Ti: sapphire regenerative amplifier (Astrella, Coherent) centered at 800 nm with a repetition rate of 1 kHz, and FWHM of ~60 nm is split into three beams. The first beam (≈1 mJ/pulse) pumps a commercial TOPAS (traveling wave optical parametric amplification of superfluorescence) coupled with an NDFG (non-collinear difference-frequency generation) unit to generate tunable mid-infrared (IR) pulses with FWHM of ~250 cm^{-1} (spectrum of IR pulse centered at 2780 cm^{-1} is shown in Fig. 2). We use a 4 f pulse shaper to produce a narrowband visible pulse (VIS, centered at about 800 nm, FWHM $\approx 10\ cm^{-1}$) from the second beam (≈0.8 mJ/pulse). IR and VIS beams are made collinear using a dichroic beam combiner. The IR/VIS pulse pair is then routed to a displaced Sagnac interferometer to generate a local oscillator (LO) by sum-frequency generation in a 10 μm thick type 1 β-barium borate (BBO) crystal. The third beam (≈1.1 mJ/pulse) is used to generate a broadband terahertz (THz) pulse by two-color mixing of laser field in air plasma (spectrum of THz pulse is shown in Fig. 2). IR, VIS, and LO pulses are focused by a parabolic mirror and overlapped with horizontally polarized terahertz (THz) pulse at the sample to generate the third-order signal. After the sample, the signal and LO are collimated with a CaF_2 lens (20 cm focal length) and passed through a polarizer. The signal and LO are aligned to a spectrometer (SpectraPro HRS-300, Princeton Instru-

ments) and detected with an electron-multiplying charge-coupled device (EMCCD) detector (Newton 971, Andor). The energies of IR and VIS pulses at the sample are 1.5 and 4.5 μJ/pulse, respectively. We use parallel polarization of THz, IR, VIS, and signal fields.

We measure time-domain data by varying the time delay between the THz and IR/VIS pulse pair in steps of 10 fs using a motorized delay stage [V-551.2B, Physik Instrumente (PI)]. The starting position of the delay stage is the same for DMSO and SiN_x membrane. We scan time delay across a total time interval of 7.33 and 1.33 ps for DMSO and SiN_x, respectively. Data acquisition for one spectrum takes about 25 min for DMSO and 5 min for the SiN_x membrane.

The sample cell for DMSO consists of a front and a back window separated by a 1 mm thick Viton o-ring. The front window is made of a 200 μm thick silicon frame with a low-stress SiN_x membrane of 50 nm thickness and 0.5 × 0.5 mm^2 aperture (NX5050A, Norcada). The back window is a 2 mm thick CaF_2 window. The 2D TIRV signal from the front window is about 30 times weaker than the DMSO signal and, thus, is neglected in data interpretation and analysis (see Fig. S5 in the supplementary material).

To measure the absorption spectrum in far- and mid-infrared, we use a commercial Fourier transform infrared (FTIR) spectrometer (Bruker Vertex 70), which has a spectral range of 50–6000 cm^{-1}. Liquid DMSO is placed between two diamond windows (400 μm thick) with a 25 μm thick PTFE spacer.

SUPPLEMENTARY MATERIAL

See the supplementary material for calibration of ω_1 and ω_2 frequencies, infrared absorption spectrum of 1 mm thick DMSO sample, and comparison of 2D TIRV signal intensity of DMSO and 50 nm thick SiN_x membrane.

ACKNOWLEDGMENTS

We acknowledge the Max Planck Society for financial support.

AUTHOR DECLARATIONS

Conflict of Interest

The authors have no conflicts to disclose.

Author Contributions

Pankaj Seliya: Data curation (lead); Formal analysis (lead); Investigation (lead); Visualization (lead); Writing – original draft (equal). **Mischa Bonn**: Formal analysis (supporting); Funding acquisition (lead); Investigation (supporting); Methodology (supporting); Project administration (supporting); Supervision (supporting); Visualization (supporting); Writing – original draft (equal). **Maksim Grechko**: Conceptualization (lead); Formal analysis (supporting); Investigation (supporting); Methodology (lead); Project administration (lead); Supervision (lead); Visualization (supporting); Writing – original draft (equal).

DATA AVAILABILITY

The data that support the findings of this study are available from the corresponding author upon reasonable request.

REFERENCES

[1] C. M. Cheatum, "Low-frequency protein motions coupled to catalytic sites," Annu. Rev. Phys. Chem. **71**, 267 (2020).
[2] H. N. Motlagh, J. O. Wrabl, J. Li, and V. J. Hilser, "The ensemble nature of allostery," Nature **508**, 331 (2014).
[3] B. Brooks and M. Karplus, "Harmonic dynamics of proteins: Normal modes and fluctuations in bovine pancreatic trypsin inhibitor," Proc. Natl. Acad. Sci. U. S. A. **80**, 6571 (1983).
[4] A. Cooper and D. T. F. Dryden, "Allostery without conformational change. A plausible model," Eur. Biophys. J. **11**, 103 (1984).
[5] M. C. Thielges, J. Y. Axup, D. Wong, H. S. Lee, J. K. Chung, P. G. Schultz, and M. D. Fayer, "Two-dimensional IR spectroscopy of protein dynamics using two vibrational labels: A site-specific genetically encoded unnatural amino acid and an active site ligand," J. Phys. Chem. B **115**, 11294 (2011).
[6] K. Kwak, S. Park, I. J. Finkelstein, and M. D. Fayer, "Frequency-frequency correlation functions and apodization in two-dimensional infrared vibrational echo spectroscopy: A new approach," J. Chem. Phys. **127**, 124503 (2007).
[7] C. J. Fecko, J. J. Loparo, S. T. Roberts, and A. Tokmakoff, "Local hydrogen bonding dynamics and collective reorganization in water: Ultrafast infrared spectroscopy of HOD/D_2O," J. Chem. Phys. **122**, 054506 (2005).
[8] B. Guchhait, C. A. Tibbetts, K. M. Tracy, B. M. Luther, and A. T. Krummel, "Ultrafast vibrational dynamics of a trigonal planar anionic probe in ionic liquids (ILs): A two-dimensional infrared (2DIR) spectroscopic investigation," J. Chem. Phys. **152**, 164501 (2020).
[9] M. L. Cowan, B. D. Bruner, N. Huse, J. R. Dwyer, B. Chugh, E. T. J. Nibbering, T. Elsaesser, and R. J. D. Miller, "Ultrafast memory loss and energy redistribution in the hydrogen bond network of liquid H_2O," Nature **434**, 199 (2005).
[10] C. J. Fecko, J. D. Eaves, J. J. Loparo, A. Tokmakoff, and P. L. Geissler, "Ultrafast hydrogen-bond dynamics in the infrared spectroscopy of water," Science **301**, 1698 (2003).
[11] M. Grechko, T. Hasegawa, F. D'Angelo, H. Ito, D. Turchinovich, Y. Nagata, and M. Bonn, "Coupling between intra-and intermolecular motions in liquid water revealed by two-dimensional terahertz-infrared-visible spectroscopy," Nat. Commun. **9**, 885 (2018).
[12] M. Grechko, S. A. Bretschneider, L. Vietze, H. Kim, and M. Bonn, "Vibrational coupling between organic and inorganic sublattices of hybrid perovskites," Angew. Chem., Int. Ed. **57**, 13657 (2018).
[13] W. Zhao and J. C. Wright, "Measurement of $X^{(3)}$ for doubly vibrationally enhanced four wave mixing spectroscopy," Phys. Rev. Lett. **83**, 1950 (1999).
[14] R. J. Falconer and A. G. Markelz, "Terahertz spectroscopic analysis of peptides and proteins," J. Infrared, Millimeter, Terahertz Waves **33**, 973 (2012).
[15] G. Acbas, K. A. Niessen, E. H. Snell, and A. G. Markelz, "Optical measurements of long-range protein vibrations," Nat. Commun. **5**, 3076 (2014).
[16] K. A. Niessen, M. Xu, D. K. George, M. C. Chen, A. R. Ferré-D'Amaré, E. H. Snell, V. Cody, J. Pace, M. Schmidt, and A. G. Markelz, "Protein and RNA dynamical fingerprinting," Nat. Commun. **10**, 1026 (2019).
[17] P. Hamm, M. Lim, and R. M. Hochstrasser, "Structure of the amide I band of Peptides measured by femtosecond nonlinear-infrared spectroscopy," J. Phys. Chem. B **102**, 6123 (1998).
[18] M. Khalil, N. Demirdöven, and A. Tokmakoff, "Obtaining absorptive line shapes in two-dimensional infrared vibrational correlation spectra," Phys. Rev. Lett. **90**, 047401 (2003).
[19] J. B. Asbury, T. Steinel, K. Kwak, S. A. Corcelli, C. P. Lawrence, J. L. Skinner, and M. D. Fayer, "Dynamics of water probed with vibrational echo correlation spectroscopy," J. Chem. Phys. **121**, 12431 (2004).
[20] J. D. Hybl, A. Albrecht Ferro, and D. M. Jonas, "Two-dimensional fourier Transform electronic spectroscopy," J. Chem. Phys. **115**, 6606 (2001).

[21] M. L. Cowan, J. P. Ogilvie, and R. J. D. Miller, "Two-dimensional spectroscopy using diffractive optics based phased-locked photon echoes," Chem. Phys. Lett. **386**, 184 (2004).
[22] S. Nihonyanagi, S. Yamaguchi, and T. Tahara, "Direct evidence for orientational flip-flop of water molecules at charged interfaces: A heterodyne-detected vibrational sum frequency generation study," J. Chem. Phys. **130**, 204704 (2009).
[23] I. V. Stiopkin, H. D. Jayathilake, A. N. Bordenyuk, and A. V. Benderskii, "Heterodyne-detected vibrational sum frequency generation spectroscopy," J. Am. Chem. Soc. **130**, 2271 (2008).
[24] L. Vietze, E. H. G. Backus, M. Bonn, and M. Grechko, "Distinguishing different excitation pathways in two-dimensional terahertz-infrared-visible spectroscopy," J. Chem. Phys. **154**, 174201 (2021).
[25] L. Vietze, M. Bonn, and M. Grechko, "Two-dimensional terahertz-infrared-visible spectroscopy elucidates coupling between low- and high-frequency modes," in *Springer Series in Optical Sciences*, edited by M. Cho (Springer, Singapore, 2019), Vol. 226, pp. 197–214.
[26] R. W. Boyd, *Nonlinear Optics*, 3rd ed. (Academic Press, Inc., 2008).
[27] M. K. Hazra and B. Bagchi, "Collective excitations in liquid dimethyl sulfoxide (DMSO): FIR spectrum, low frequency vibrational density of states, and ultrafast dipolar solvation dynamics," J. Chem. Phys. **146**, 024505 (2017).
[28] W. D. Horrocks and F. A. Cotton, "Infrared and Raman spectra and normal Coordinate analysis of dimethyl sulfoxide and dimethyl sulfoxide-d_6," Spectrochim. Acta **17**, 134 (1961).
[29] P. P. Wiewiór, H. Shirota, and E. W. Castner, "Aqueous dimethyl sulfoxide solutions: Inter- and intra-molecular dynamics," J. Chem. Phys. **116**, 4643 (2002).
[30] G. Cataldo, J. A. Beall, H.-M. Cho, B. McAndrew, M. D. Niemack, and E. J. Wollack, "Infrared dielectric properties of low-stress silicon nitride," Opt. Lett. **37**, 4200 (2012).
[31] K. C. Lin and S. C. Lee, "The structural and optical properties of a-SiN_x:H Prepared by plasma-enhanced chemical-vapor deposition," J. Appl. Phys. **72**, 5474 (1992).